

Skeleton kinetic model of acetaldehyde oxidation from comprehensive models

C.H. Liang^a, C.Y. Mou^a, D.J. Lee^{b,*}

^aDepartment of Chemistry, National Taiwan University Taipei, 10617, Taiwan

^bDepartment of Chemical Engineering, National Taiwan University Taipei, 10617, Taiwan

Received 4 December 2003; received in revised form 15 September 2004; accepted 5 November 2004

Available online 28 January 2005

Abstract

This work elucidated the chemical reaction scheme developed by Wang and Mou (Wang–Mou scheme) in 1985 for describing the dynamic behavior of acetaldehyde oxidized in a continuous-flow stirred tank reactor (CSTR). We deduced the Wang–Mou scheme from the more comprehensive chemical reaction schemes proposed by previous literature works (detailed scheme), and the correlation between the detailed scheme and the Wang–Mou scheme was established. Numerical simulation was adopted to explore the dynamic characteristics of the Wang–Mou scheme and compared with the experiments, revealing a reasonable agreement with the experimental findings. Finally, mechanisms responsible for various dynamic regimes were discussed. The link of the skeleton, Wang–Mou scheme, with the more comprehensive schemes was established.

© 2005 Elsevier Ltd. All rights reserved.

Keywords: Skeleton model; Wang–Mou model; Acetaldehyde; Oscillations

1. Introduction

The chemical reaction of an equimolar mixture of acetaldehyde and oxygen in a continuous-flow stirred tank (CSTR) can generate various dynamic behaviors, including steady-states, bi-stability, cool-flame oscillations, ignition oscillation, and complex ignition–cool flame oscillations (Gray et al., 1981a, b). These experimental findings have been interpreted using detailed chemical analyses (Halstead et al., 1971, 1973, Felton et al., 1976; Gibson et al., 1984; Kaiser et al., 1986; Pugh et al., 1987; Westbrook and Dryer, 1984; Harrion and Cairine, 1988; Griffiths and Sykes, 1989; Cavanagh et al., 1990; Di Mao et al., 1993). For instance, the model proposed by Felton et al. (1976) described the cool-flame oscillation phenomena. Furthermore, the 25 elementary reactions proposed by Gibson et al. (1984) allowed

the complex ignition oscillation sequence to be generated, while Kaiser et al. (1986) proposed a scheme involving 153 elementary reactions.

To provide a theoretical framework in order to understand in detail the acetaldehyde oxidation system, Yang and Gray (1969a, b) presented a two-variable (the autocatalytic chain carrier and the pool temperature) skeleton model that combined chain-branching mechanisms during combustion and Salnikoff's thermokinetic theory (Scott, 1991). However, the Yang–Gray model cannot generate the complex ignition oscillation patterns observed in experiments (Gray et al., 1981a, b) and in simulations with detailed kinetics (Gibson et al., 1984). Wang and Mou (1985) modified the Yang–Gray model by considering fuel consumption and adding a high temperature branching step. Griffiths (1995) comprehensively reviewed the literature on skeleton kinetic models.

The Wang–Mou model displays the dynamic behaviors of acetaldehyde oxidation system. Based on the works by Halstead et al. (1971, 1973), Gibson et al. (1984) and

* Corresponding author. Tel.: +886 2 363 5230; fax: +886 2 2362 5632.
E-mail address: djlee@ccms.ntu.edu.tw (D.J. Lee).

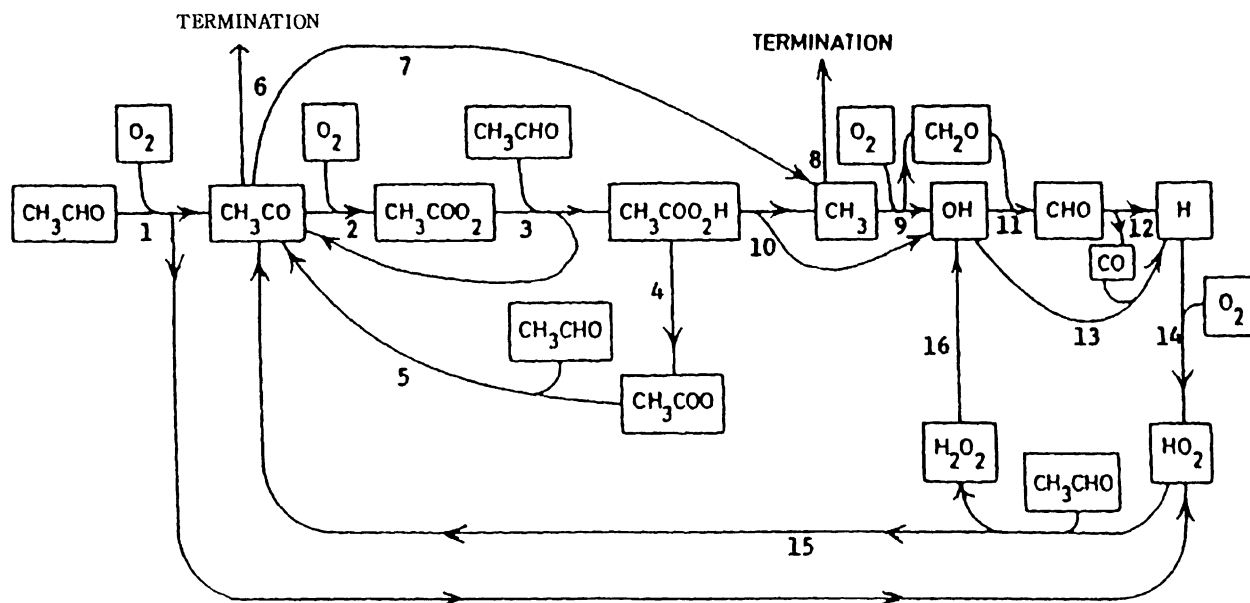


Fig. 1. The Wang–Mou scheme for acetaldehyde oxidation. Numbers indicate the elementary reactions listed in Table 2.

Vardanyan and Nalbandydn (1985), Wang and Mou proposed a detailed chemical kinetic scheme, presented in Fig. 1 and referred to as the “Wang–Mou scheme” herein, and noted its correspondence with the three-variable, skeleton model. Liang et al. (2003) demonstrated the new bifurcation regimes of Wang–Mou model and identified the significant kinetic parameters on the system’s dynamics. The model output agreed qualitatively with the experimental findings.

In numerical simulation of a complex chemical reaction system in chemical reactor, skeleton mechanisms are often used in place of detailed chemistry since comprehensive chemical kinetics can involve too many species and reactions to be considered in calculations. For instance, with skeleton models for oscillatory reactions, the effects of non-ideal mixing in the flow reactor were demonstrated (Hsu et al., 1994, 1996, Chang et al., 1996, 1999). The manner in dispute is whether the skeleton model can represent the real system of comprehensive scheme (Lee et al., 1997; Sirdeshpande et al., 2001; Banerjee and Ierapetritou, 2003). The link between skeleton model and comprehensive chemical model remains unclear to most complex chemical system.

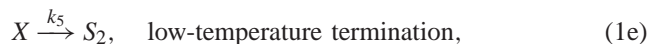
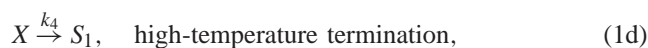
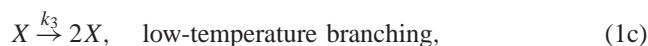
This study demonstrated that the Wang–Mou scheme could be satisfactorily deduced from a more comprehensive scheme like the one proposed in Kaiser et al. (1986). We first briefly summarized the Wang–Mou model and the related chemical reactions in Section 2. Then, the Wang–Mou scheme was deduced with modification from the Kaiser et al.’s scheme and other works. Subsequently, Section 3 conducted numerical simulations of the Wang–Mou scheme, and the simulation results were compared with experimental findings. Section 4 discussed the theoretical findings, and

finally conclusions were presented in Section 5. With the present study the skeleton Wang–Mou scheme is linked to the comprehensive model, hence can be used in modeling processes incorporating other factors, such as the role of macromixing or micromixing on the chemical dynamics of acetaldehyde oxidation.

2. Reaction scheme and model deduction

2.1. Reaction model

The Wang–Mou model is as follows:



where $f = 2$ in this work. The rate constants, k_i ’s, have Arrhenius-forms, whose activation energy E_i ’s follow the pattern $E_2 > E_1 > E_4 > E_3 > E_5$. Additionally assume that the reactor is a perfectly mixed (CSTR) with a residence time of $\tau = 1/k_f$ and adopts Newtonian cooling, then the following mass and energy balance equations can be obtained:

$$\frac{dx}{dt} = k_1Y + k_2xY - (k_5 + k_4 - k_3)x - x, \quad (2a)$$

Table 1
Kinetic scheme and the kinetic parameters^a for acetaldehyde oxidation

No.	Reaction	A (s ⁻¹ cm ³ , mol ⁻¹ s ⁻¹ , or cm ⁶ mol ⁻² s ⁻¹)	E (kJ/mol)	ΔH _{298 K} (kJ/mol)
W1	CH ₃ CHO + O ₂ → CH ₃ CO + HO ₂	3.0 × 10 ¹²	106	164
W2	CH ₃ CO + O ₂ → CH ₃ CO ₃	2.0 × 10 ¹¹	0	-288
W3	CH ₃ CO ₃ + CH ₃ CHO → CH ₃ CO ₃ H + CH ₃ CO	1.0 × 10 ¹³	42	-50
W4	CH ₃ CO ₃ H → CH ₃ CO ₂ + OH	4.0 × 10 ¹³	167	125.5
W5	CH ₃ CO ₂ + CH ₃ CHO → CH ₃ CO ₂ H + CH ₃ CO	2.0 × 10 ¹³	42	-90
W6	CH ₃ CO $\xrightarrow{\text{wall}}$ termination	3.3 × 10 ³	0	0
W7	CH ₃ CO \xrightarrow{M} CH ₃ + CO	2.0 × 10 ¹⁶	63	66.9
W8	2CH ₃ → C ₂ H ₆	2.5 × 10 ¹³	0	-360
W9	CH ₃ + O ₂ → CH ₂ O + OH	3.2 × 10 ¹³	83.14	-293
W10	CH ₃ CO ₃ H → CH ₃ + CO ₂ + OH	3.2 × 10 ¹⁵	180	247
W11	CH ₂ O + OH → CHO + H ₂ O	3.2 × 10 ¹⁰	0	-132.6
W12	CHO \xrightarrow{M} CO + H	1.5 × 10 ¹⁴	79.42	70.4
W13	CO + OH → CO ₂ + H	3.0 × 10 ¹¹	2.51	-104.2
W14	H + O ₂ \xrightarrow{M} HO ₂	5.0 × 10 ¹²	-5.43	-197.3
W15	HO ₂ + CH ₃ CHO → CH ₃ CO + H ₂ O ₂	1.2 × 10 ¹²	33.26	-346
W16	H ₂ O ₂ \xrightarrow{M} 2OH	3.1 × 10 ¹⁷	194.6	210

^aKinetic data are extracted from Bensen (1960), Kerr and Dickson (1961), Felton et al. (1976), Halstead et al. (1973), Basco (1972), Baker et al. (1970), NSRDS-NBS 67 (1980), and NSRDS-NBS 37 (1971).

$$\frac{dY}{dt} = -k_1Y - k_2xY + 1 - Y, \quad (2b)$$

$$\frac{dU}{dt} = k_1h_1Y + (k_2h_2Y + k_3h_3 + k_4h_4 + k_5h_5)x - k_Tx. \quad (2c)$$

Notably, let $k_2 = 0$ then Eqs. (2a–c) reduce to the original Yang–Gray model.

Table 1 lists the chemical reactions of the Wang–Mou scheme. As proposed in Wang and Mou (1985), reaction (W1) denotes the initiation step; reactions (W2–W5), the low-temperature branching; reaction (W6), the low-temperature termination; reactions (W7) and (W8), the high-temperature termination; and reactions (W7) and (W9–W16), the high-temperature branching stage. The scheme proposed by Kaiser et al. (1986) comprises 153 elementary reactions, among which 41 are claimed to be significant over the temperature range 550–900 K. Table 2 lists the 41 significant reactions proposed therein, which are numbered herein as in the original paper. For instance, Eq. (K2) refers to Eq. (2) in Kaiser et al.'s paper.

2.2. Model deduction

2.2.1. Initiation step

The initiation step was proposed as the formation of the acetyl radical CH₃ĊO according to the following kinetics (Gibson et al., 1984):

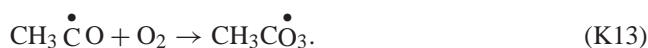


The corresponding activation energy is 170 kJ/mol and the reaction rate is expected to be low. Eq. (K2) correlates with

Eqs. (1a) and (W1) in Table 2, while CH₃ĊO closely corresponds to variable x in Wang–Mou's model.

2.2.2. Low-temperature branching step

Using the experimental data of Blanchard et al. (1957), Halstead et al. (1971, 1973) demonstrated that CH₃CO₃H is the branching agent. Meanwhile, Gray et al. (1981a, b) confirmed that CH₃CO₃H is the major intermediate of cool flames. The low-temperature branching step should thus comprise the conversion of CH₃ĊO₂ to CH₃CO₃H at low-activation energy, listed as follows:



Initially, the concentration of free radicals should be significantly less than [CH₃CHO]. Consequently, the CH₃ĊO₃ formed by this reaction mainly reacts with the CH₃CHO, as follows:



Consequently, steps K14 and K17–K20 can be ignored.

Experimental findings indicate the existence of CH₃COOH in acetaldehyde oxidation. Furthermore, the reaction between CH₃ĊO₂ and CH₃CHO is an H-abstraction reaction, with relatively low-activation energy. Consequently, the subsequent low-temperature branching reactions are proposed to be as follows:



Table 2

The 41 significant elementary reactions proposed by Kaiser et al. (1986) during 550–900 K for oxidation of acetaldehyde

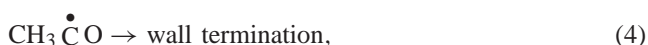
No.	Reaction	Log A*	n(-)	E _a (kcal/mol)
K2	CH ₃ CHO + O ₂ → CH ₃ CO + HO ₂	13.3	0	42.20
K3	CH ₃ CHO + H → CH ₃ CO + H ₂	13.6	0	4.2
K4	CH ₃ CHH + OH → CH ₃ CO + H ₂ O	13.0	0	0
K6	CH ₃ CHO + HO ₂ → CH ₃ CO + H ₂ O ₂	12.23	0	10.70
K7	CH ₃ CHO + CH ₃ → CH ₃ CO + CH ₄	12.24	0	8.44
K8	CH ₃ CHO + CH ₃ CO ₃ → CH ₃ CO + CH ₃ CO ₃ H	11.08	0	4.90
K9	CH ₃ CHO + CH ₃ O → CH ₃ CO + CH ₃ OH	11.06	0	1.28
K10	CH ₃ CHO + CH ₃ O ₂ → CH ₃ CO + CH ₃ O ₂ H	9.55	0	5.05
K12	CH ₃ CO \xrightarrow{M} CH ₃ + CO	16.26	0	14.40
K13	CH ₃ CO + O ₂ → CH ₃ CO ₃	10.00	0	-2.70
K14	CH ₃ CO ₃ + HO ₂ → CH ₃ CO ₃ H + O ₂	12.00	0	0
K15	CH ₃ CO ₃ H → CH ₃ CO ₂ + OH	15.60	0	40.00
K17	CH ₃ CO ₃ + CH ₃ O ₂ → CH ₃ CO ₂ + CH ₃ O + O ₂	12.26	0	0
K18	CH ₃ CO ₃ + CH ₃ O ₂ → CH ₃ CO ₂ H + CH ₂ O + O ₂	11.48	0	0
K19	CH ₃ CO ₃ + HO ₂ → CH ₃ CO ₂ + OH + O ₂	12.00	0	0
K20	CH ₃ CO ₃ + CH ₃ CO ₃ → CH ₃ CO ₂ + CH ₃ CO ₂ + O ₂	12.68	0	0
K21	CH ₃ CO ₂ \xrightarrow{M} CH ₃ + CO ₂	16.26	0	14.40
K22	CH ₃ O ₂ + HO ₂ → CH ₃ O ₂ H + O ₂	10.66	0	-2.60
K23	CH ₃ O ₂ + CH ₃ → CH ₃ O + CH ₃ O	12.58	0	-1.20
K24	CH ₃ O ₂ + HO ₂ → CH ₃ O + OH + O ₂	12.00	0	0
K25	CH ₃ O ₂ + CH ₃ O ₂ → CH ₂ O + CH ₃ OH + O ₂	11.26	0	0
K26	CH ₃ O ₂ + CH ₃ O ₂ → CH ₃ O + CH ₃ O + O ₂	12.57	0	2.20
K29	CH ₃ O ₂ H → CH ₃ O + OH	14.81	0	43.0
K30	CH ₃ O ₂ H + OH → CH ₃ O ₂ + H ₂ O	13.51	0	1.00
K31	CH ₃ O ₂ H + OH → CH ₂ O ₂ H + H ₂ O	13.40	0	1.00
K41	CH ₃ OH + OH → CH ₂ OH + H ₂ O	12.60	0	1.37
K47	CH ₃ OH + OH → CH ₃ O + H ₂ O	13.09	0	3.25
K49	CH ₂ OH + O ₂ → cH ₂ O + HO ₂	11.92	0	0
K54	H + O ₂ \xrightarrow{M} HO ₂	15.22	0	-1.00
K63	HO ₂ + HO ₂ → H ₂ O ₂ + O ₂	11.11	0	-1.24
K72	HCO + O ₂ → CO + HO ₂	12.48	0	0
K79	CH ₂ O + OH → HCO + H ₂ O	12.88	0	0.17
K82	CH ₂ O + HO ₂ → HCO + H ₂ O ₂	11.30	0	8.00
K83	CH ₂ O + CH ₃ O → HCO + H ₂ O ₂	11.06	0	1.28
K86	CH ₂ O + CH ₃ → HCO + CH ₄	10.00	0.5	6.00
K87	CH ₃ O \xrightarrow{M} CH ₂ O + H	13.70	0	21.00
K88	CH ₃ O + O ₂ → CH ₂ O + HO ₂	10.88	0	2.70
K100	CH ₃ + HO ₂ → CH ₃ O + OH	13.51	0	0
K101	CH ₃ + O ₂ \xrightarrow{M} CH ₃ O ₂	16.15	0	-1.10
K102	CH ₃ + CH ₃ → C ₂ H ₆	13.40	0	0
K153	CH ₂ O ₂ H → CH ₂ O + OH	15.60	0	23.00

Rate constant $k = AT^n \exp(-E_a/RT)$. Units for A are in cm³, mol, s, and kcal.

The decomposition of CH₃ĊO₂ is more significant at high temperatures, reaction K21 is neglected in the low-temperature branching step. Consequently, the low-temperature branching step should comprise Eqs. (K8), (K13), (K15), and (3), which correspond to Eqs. (W2–W5) in Table 2.

2.2.3. Low-temperature termination step

According to Yang and Gray (1981a), the wall reaction with CH₃ĊO should correspond to the low-temperature termination step. Namely,



with null activation energy. Eq. (W6) in Table 2 correlates with this equation.

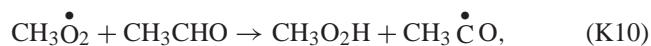
2.2.4. High-temperature termination step

Wang and Mou (1985) proposed the high-temperature termination reactions to be



and other reactions that remove ĊH₃. Meanwhile, Gibson et al. (1984) speculated that the following reactions should

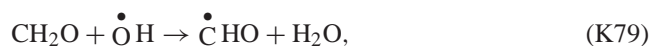
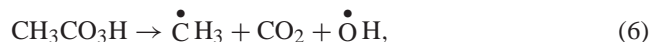
contribute to the low-temperature branching:



Since $\text{CH}_3\text{O}_2\text{H}$ is a relatively stable species, reaction (K29) is unlikely to be involved in high-temperature termination step. Furthermore, $\dot{\text{C}}\text{H}_3$ is the product of high-temperature decomposition, and its concentration should be relatively low in cool flames. Consequently, the reactions following (K101) in acetaldehyde oxidation should be negligible, including Eqs. (K10), (K22)–(K26), (K29)–(K31), (K41), (K47), (K49), (K83), (K87), (K88), and (K153).

2.2.5. High-temperature branching step

Gray et al. (1981a, b) confirmed that both CH_2O and H_2O_2 are products of cool flames, and induce further thermal ignition and subsequent high-temperature branching. Meanwhile, Halstead et al. (1971, 1973) demonstrated that $\dot{\text{O}}\text{H}$ radicals are essential species for high-temperature ignition. Following from these observations, the following steps are proposed herein for high-temperature branching:



Relatively small amounts of $\dot{\text{C}}\text{H}_3$ radicals are formed in the initial phase of ignition, while $[\text{HO}_2] \ll [\text{O}_2]$, and thus reactions (K100) and (K9) should be insignificant. Most HO_2 radicals are formed through chain branching of $\dot{\text{C}}\text{H}_3$ through reaction (K54). Following the formation of CH_2O the concentration of HO_2 would be minimized, and reaction (K82) can thus be neglected. The $\dot{\text{H}}$ radicals react mainly with O_2 to form HO_2 , which negates the role of reaction (K3). The main products of high-temperature branching are CO_2 and H_2O , along with which the formation of CH_4 is insignificant. Hence, reactions (K86) and (K7) are not significant. The $\dot{\text{C}}\text{HO}$ ions can only be decomposed at a high temperature to form $\dot{\text{H}}$, and reaction (K54) is thus more important than (K72), making the latter is negligible.

Reactions (K4) and (K63) may be important to the high-temperature branching step. Reactions controlling the high-temperature branching should display high activation energy and a high heat release rate (Wang and Mou, 1985). The heat of reaction (K6) is 346 kcal/mol, while that of (K4) and (K63) is 59 and 178 kcal/mol, respectively. Consequently, the latter two reactions can be neglected. Owing to the important role of $\dot{\text{O}}\text{H}$ radicals in high-temperature branching as proposed by Halstead et al. (1971, 1973), and the requirement that the dominating reaction has high activation energy, reaction (9) is included as an essential step, whose activation energy is 210 kcal/mol.

Apparently, Eqs. (K2), (K8), (K15), (3), (4), (K12), (K102), (5), (6), (K79), (7), (8), (K54), (K6) and (9) correspond to Eqs. (W1–W16) in Table 2. The Wang–Mou scheme has been deduced from the comprehensive scheme by Kaiser et al. (1986) and also from other works. As proposed by Wang and Mou (1985), reaction (K2) denotes the initiation; reactions (3), (K8), (K13) and (K15) are the low-temperature branching steps; reaction (4) is the low-temperature termination step; reactions (K12) and (K102) are high-temperature termination steps, while high-temperature branching comprises reactions (5–9), (K6), (K54) and (K79).

3. Numerical simulation

3.1. Equations and solution

The chemical scheme listed in Table 1 comprises 16 elementary reactions and 19 variables (18 chemical species and temperatures). The mass balances in a perfect CSTR are as follows:

$$\frac{d[x_j]}{dt} = \sum_{i,j,k} k_i [x_j][x_k] + \frac{1}{\tau} ([x_j]_0 - [x_j]), \quad (10)$$

where i represents the i th elementary reaction ($i = 1$ –16), and j and k denote the chemical species (1–18). Meanwhile, $[x_j]_0$ represents the concentration in the feed. The present simulations only contain O_2 and CH_3CHO . We set $[\text{O}_2]_0 = [\text{CH}_3\text{CHO}]_0 = P/(2 \times 760 \times 82 \times T_0) = N_0/2$, where N_0 is the concentration (mol/cm^3). The energy equation is

$$\frac{dU}{dt} = \sum_{i,j,k} \frac{k_j}{C} (-\Delta H_i) [x_j][x_k] - \frac{k_T}{C} u, \quad (11)$$

where C denotes the specific heat ($=11N_0 \text{ cal}/\text{cm}^3 \text{ K}$) and k_T represents the constant of Newton's cooling law, taking the same value as in Wang and Mou (1985) ($0.000368 \text{ cal}/\text{s cm}^3 \text{ K}$).

Eqs. (10) and (11) are solved simultaneously using the Gear method with $P = 100$ torrs and $\tau = 4$ s. Meanwhile, the kinetic constants listed in Table 1 are employed throughout this work.

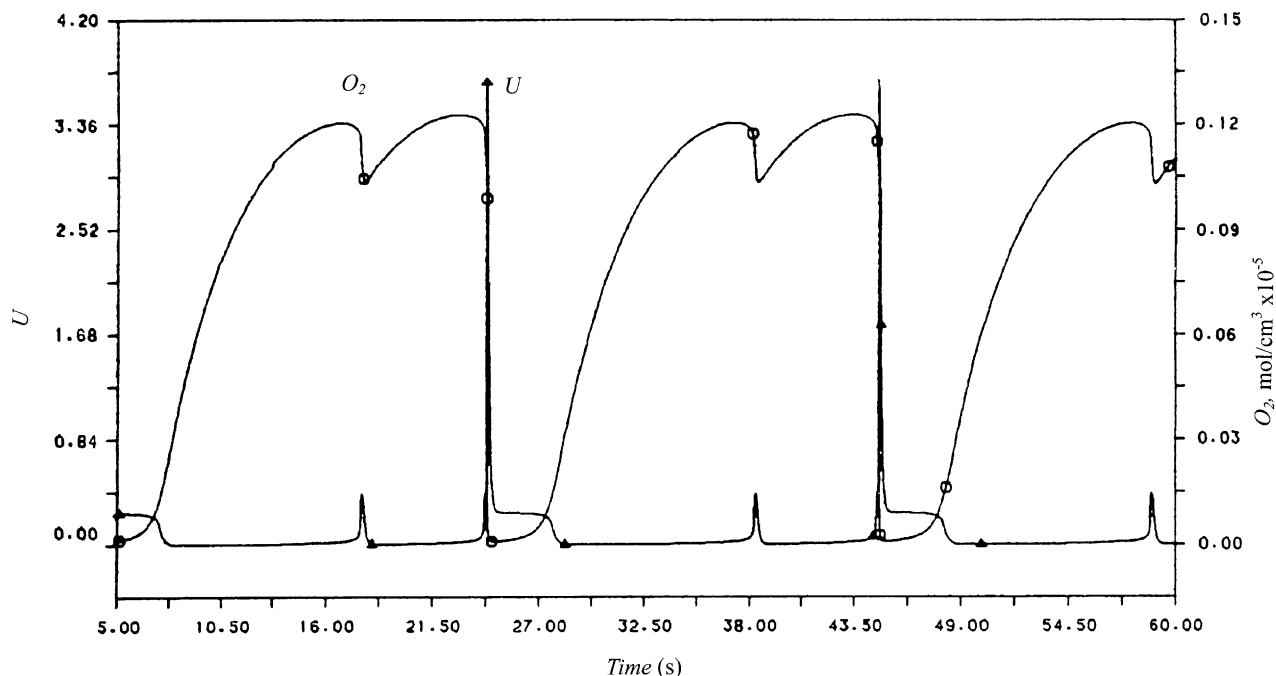


Fig. 2. Time evolutions of U and concentration of O_2 in oscillatory state P_1^1 . Regime III. $P = 100$ Torr, $T_0 = 577.8$ K, $\tau = 4$ s.

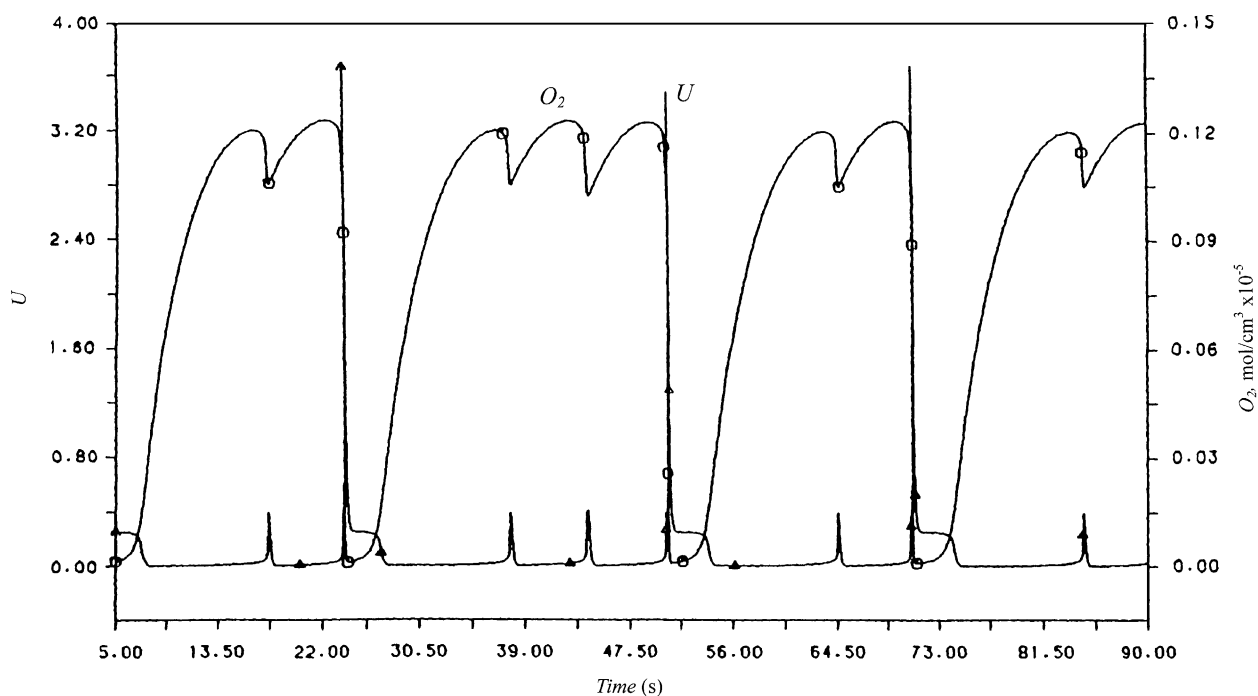


Fig. 3. Time evolutions of U and concentration of O_2 in chaotic state $C_1^{1,3}$. Regime III. $P = 100$ Torr, $T_0 = 578$ K, $\tau = 4$ s.

The five regimes of distinct chemical dynamics are noted in simulations, in which the following boundaries are identified: I–II, 555 K; II–III, 577.8 K; III–IV, 578.5 K, and IV–V, 597 K, respectively. Consequently, the T_0 for IV–V is less than that from the Wang–Mou model, which better fits the experimental data (approximately 600 K). The T_0 at I–II and

II–III boundaries are 50 and 30 K greater than the experimental results, indicating that the oscillation range predicted by simulations is still somewhat narrower than in the experiments. Figs. 2 and 3 illustrate the P_1^1 and $C_1^{1,2}$ oscillations in Regime III. More complicated sequences can be obtained by dividing T_0 more finely.

Table 3

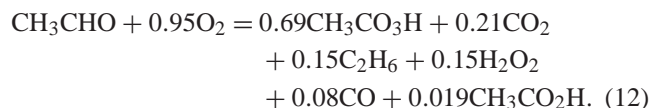
The concentrations of species at the low-temperature (550 K) and the high-temperature steady state (640 K)

	CH ₃ CHO	O ₂	CH ₃ CO	HO ₂	CH ₃ CO ₃	CH ₃ CO ₃ H
550 K	1.38255 × 10 ⁻⁶	1.38611 × 10 ⁻⁶	5.55450 × 10 ⁻¹⁴	2.30540 × 10 ⁻¹²	1.0050 × 10 ⁻¹¹	5.52510 × 10 ⁻⁸
640 K	9.99427 × 10 ⁻⁷	1.05264 × 10 ⁻⁶	9.15037 × 10 ⁻¹⁴	1.13724 × 10 ⁻¹¹	4.2515 × 10 ⁻⁸	1.12558 × 10 ⁻⁹
	CH ₃ CO ₂	OH	CH ₃ CO ₂ H	CH ₃	CO	C ₂ H ₆
550 K	1.17168 × 10 ⁻¹³	2.08090 × 10 ⁻¹²	1.42849 × 10 ⁻⁹	1.06023 × 10 ⁻¹¹	6.15092 × 10 ⁻⁹	1.12097 × 10 ⁻⁸
640 K	2.34230 × 10 ⁻¹¹	1.01730 × 10 ⁻¹²	8.48927 × 10 ⁻⁹	3.48930 × 10 ⁻¹¹	1.00160 × 10 ⁻⁷	1.21733 × 10 ⁻⁷
	CH ₂ O	CO ₂	CHO	H ₂ O	H	H ₂ O ₂
550 K	2.18900 × 10 ⁻¹¹	1.63150 × 10 ⁻⁸	9.99060 × 10 ⁻¹⁴	5.80140 × 10 ⁻¹⁴	3.38271 × 10 ⁻¹¹	1.12337 × 10 ⁻⁸
640 K	1.08600 × 10 ⁻⁹	1.44617 × 10 ⁻⁷	1.81770 × 10 ⁻¹³	1.30325 × 10 ⁻¹⁰	5.37620 × 10 ⁻¹⁰	1.22635 × 10 ⁻⁷

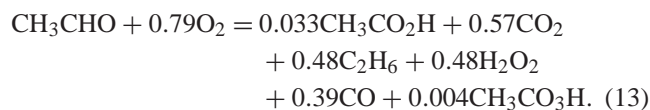
Concentrations are in mol/cm³.

3.2. Stationary states: Regimes I and V

Table 3 lists the concentrations of the 18 species in Regimes I and V. Notably, the major products in Regime I (550 K) are CH₃CO₃H, C₂H₆, CO₂, H₂O₂, CO, and CH₃CO₂H, and a small amount of H₂O. The stoichiometric balance of C, H and O is as follows:



Meanwhile, in Regime V (640 K) the major products are CO, CO₂, H₂O₂, C₂H₆, a small amount of CH₃CO₂H, and a trace of CH₃CO₃H. The stoichiometric balance equation of C, H and O is as follows:



In this regime the concentration of CH₃CO₃H is rather low, while CO increases markedly. Although the concentration of H₂O is much greater in Regime V than in Regime I, it remains negligible in practice.

As mentioned above, in both Regimes I and V, with the exception of the formation of H₂O, the model output correlates well with the experimental results (Gray et al., 1981a, b).

3.3. Cool flames and two-stage ignition

Figs. 4a–c display the variations of temperature in Regimes II–IV, respectively. The rise in temperature is around 120 K with cool flames (Fig. 4a), which correlates with the behavior for the first stage of the two-stage ignition in Regime II. In both Regimes III and IV, the rise in temperature can exceed 1500 K following fuel ignition (Figs. 4b and c). Meanwhile, after ignition a long tailing period occurs in which the temperature slowly declines. No such tailing regime is noted after the cool flame, as shown in Fig. 4a.

According to Fig. 5a (Regime II), the change in CH₃CHO concentration correlates closely with the evolution of

pool temperature. In the cool flame regime before ignition, large amounts of CH₃CHO are produced through reaction (1). When [CH₃CHO] peaks, ignition occurs. After ignition the concentration of CH₃CHO rapidly reduces to a local minimum value according to reactions (6) and (7). Most CH₃CHO and O₂ was exhausted following ignition. Before being completely depleted the residual CH₃CHO and O₂ yield a small peak of CH₃CHO concentration that produces the tailing regime. Meanwhile, the complete exhaustion of CH₃CHO brings the pool temperature back to T₀. In a cool flame regime (Fig. 5b) no small peak of CH₃CHO as noted above had appeared, corresponding to the absence of the tailing regime. Results presented in Figs. 5a and b confirm that CH₃CHO correlates with the species *x* in the Wang–Mou model.

Figs. 6a–d illustrate the evolutions of H₂O₂, CO₂, CO, CH₂O, CH₃CO₃H, O₂ and temperature in the cool flame regime (590 K). The initiation step (reaction 1) occurs when CH₃CO₃H and O₂ are fed into the CSTR. Since the activation energy is rather high, CH₃CHO and HO₂ are both generated at low concentrations. According to reactions (2) and (3) in the Wang–Mou scheme the concentration of CH₃CO₃H reaches its peak following the maximum of O₂ (Fig. 6b). After the maxima of CH₃CO₃H and O₂ the peak temperature occurs, followed by the maxima of C₂H₆, CO₂, H₂O and CH₃CO₂H. Meanwhile, CH₃ concentration reaches its maximum before the occurrence of cool flame. Therefore, Eqs. (W1–W8) help facilitate the occurrence of cool flame, while the maximum [CH₃CO₃H] triggers its occurrence.

Fig. 6c reveals that both H₂O₂ and CHO appear after the peak temperature. The pool temperature is initially low, where HO₂ has reached its maximum. As cool flame occurs and causes the temperature to rise, the concentration of CH₃CHO has not yet reached its lowest level, and reaction (W15) thus has an opportunity to proceed. The consequence of this phenomenon is to further reduce [CH₃CHO] to a minimum value, and to generate large amounts of H₂O₂. Additionally, higher pool temperature increases the speed at which reaction (W9) generates CH₂O. The main products of

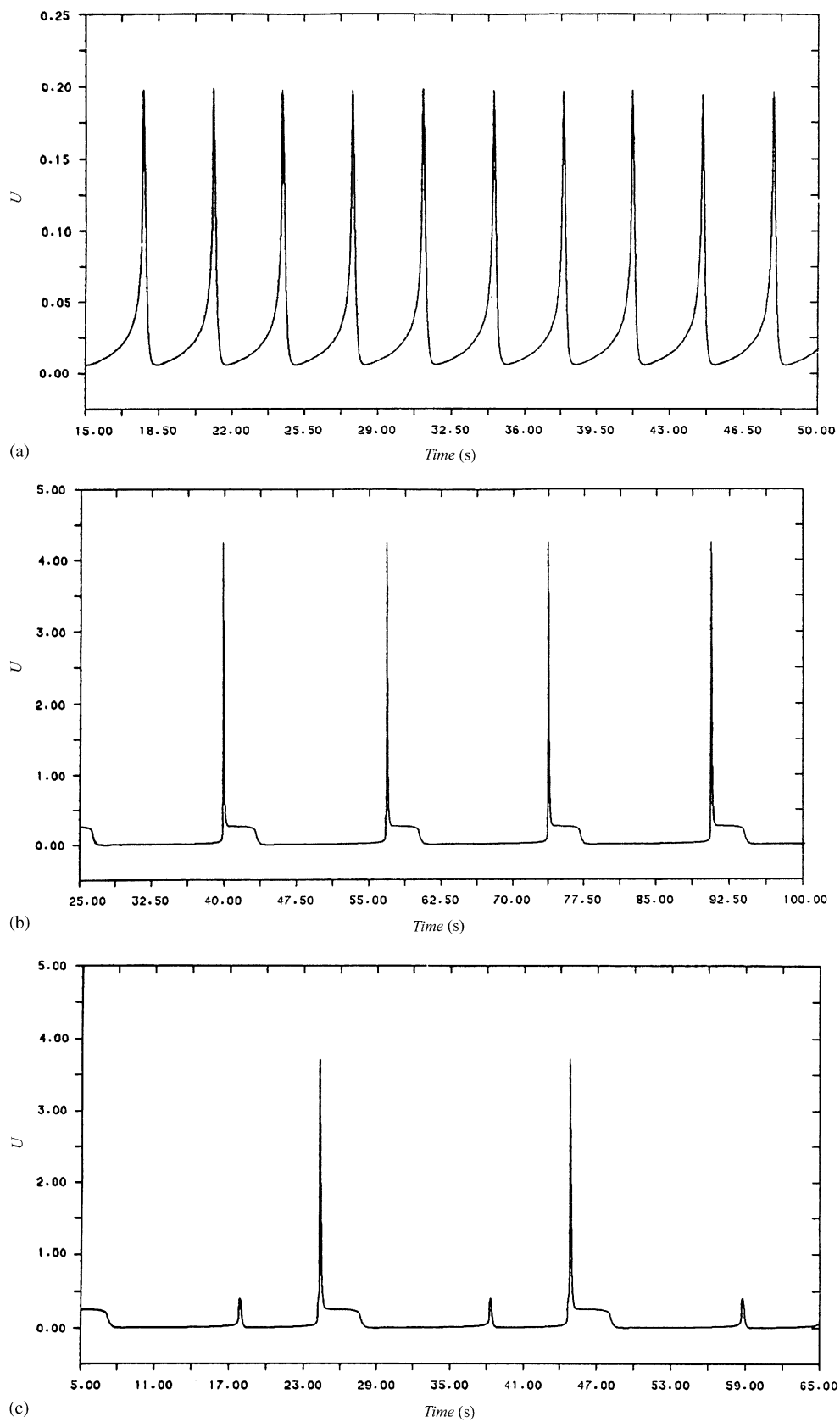


Fig. 4. Time evolutions of U at $P = 100$ Torr, $\tau = 4$ s: (a) $T_0 = 590$ K (Regime IV), (b) $T_0 = 570.0$ K, two-stage ignition (Regime II), (c) $T_0 = 577.8$ K, complex oscillation (Regime III).

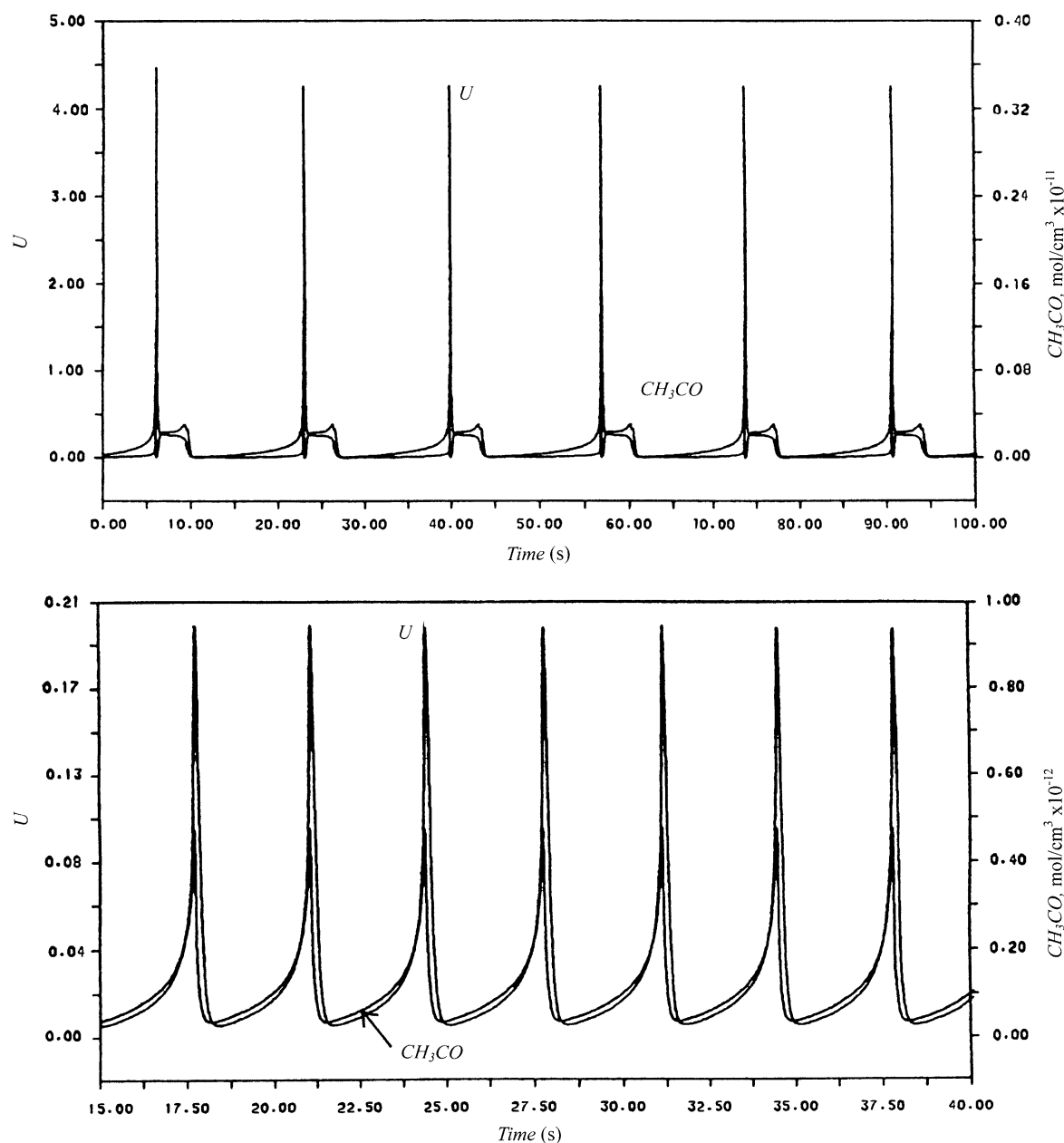


Fig. 5. Time evolutions of U and concentration of CH_3CO at $P = 100$ Torr, $\tau = 4$ s: (a) $T_0 = 570$ K (Regime II), (b) $T_0 = 590$ K (Regime IV).

the cool flame are thus CH_2O and H_2O_2 , both of which are generated after the cool flame. Fig. 6d displays that CO is exhausted through reaction (W13) when cool flame occurs, which produces large quantities of CO_2 . Simulation results reveal that the residual O_2 and CH_3CHO exceed 50%, which suggests an incomplete combustion in the cool flame.

Figs. 7a–d display the evolutions of chemical species corresponding to the two-stage ignition. Initially, reaction (W1) generates a small amount of $\dot{\text{H}}\text{O}_2$. Subsequently the cool flame occurs according to reactions (W2–W8), accompanied with which the local maximum of H_2O_2 appears using reaction (W15). A peak of $[\dot{\text{O}}\text{H}]$ occurs according to reaction (W16) before ignition. Meanwhile, after the cool flame

the $\dot{\text{C}}\text{H}_3$ radicals are converted into CH_2O and $\dot{\text{C}}\text{H}\text{O}$ using reactions (W9) and (W10), which yield maximum concentrations of these two species. The induction period between the cool flame and ignition is rather short, and consequently reactions (W9), (W11) and (W16) proceed rapidly after the cool flame which maximize the concentrations of $\dot{\text{H}}\text{O}$, CH_2O and $\dot{\text{C}}\text{H}\text{O}$. This action ignites the fuel. As Fig. 7c shows, CH_2O is exhausted almost immediately following ignition, indicating that CH_2O is the precursor of thermal ignition. Meanwhile, the maximum concentration of CO_2 occurs after ignition (Fig. 7d), while the concentration of CO declines to a minimum value. Apparently, reactions (W12) and (W13) proceed immediately after ignition, and the maximum

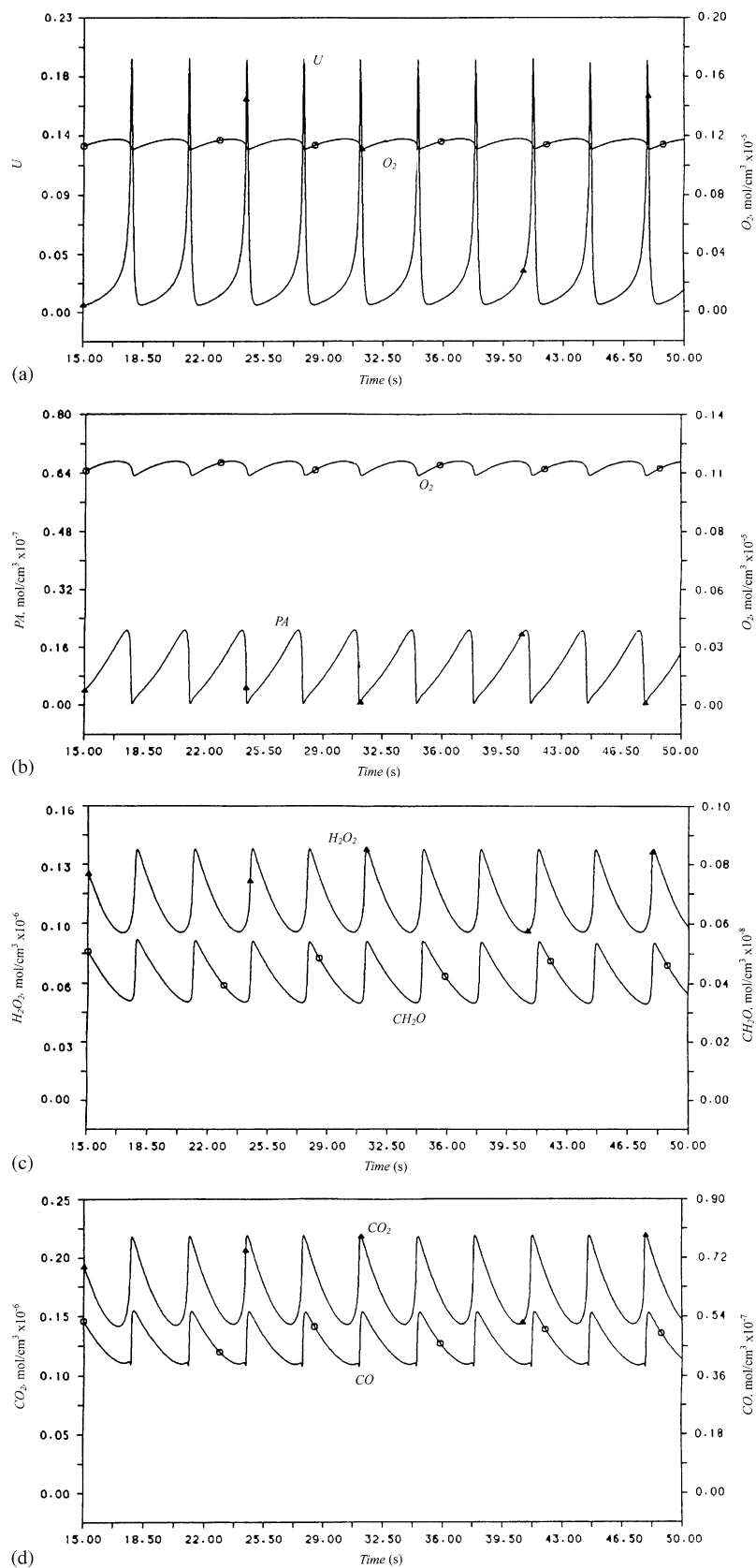


Fig. 6. Time evolutions of temperature and species at $P=100$ Torr, $T_0=590$ K and $\tau=4$ s (Regime IV): (a) U and concentration of O_2 , (b) concentrations of O_2 and peracetic acid, (c) concentrations of H_2O_2 and CH_2O , (d) concentrations of CO and CO_2 .

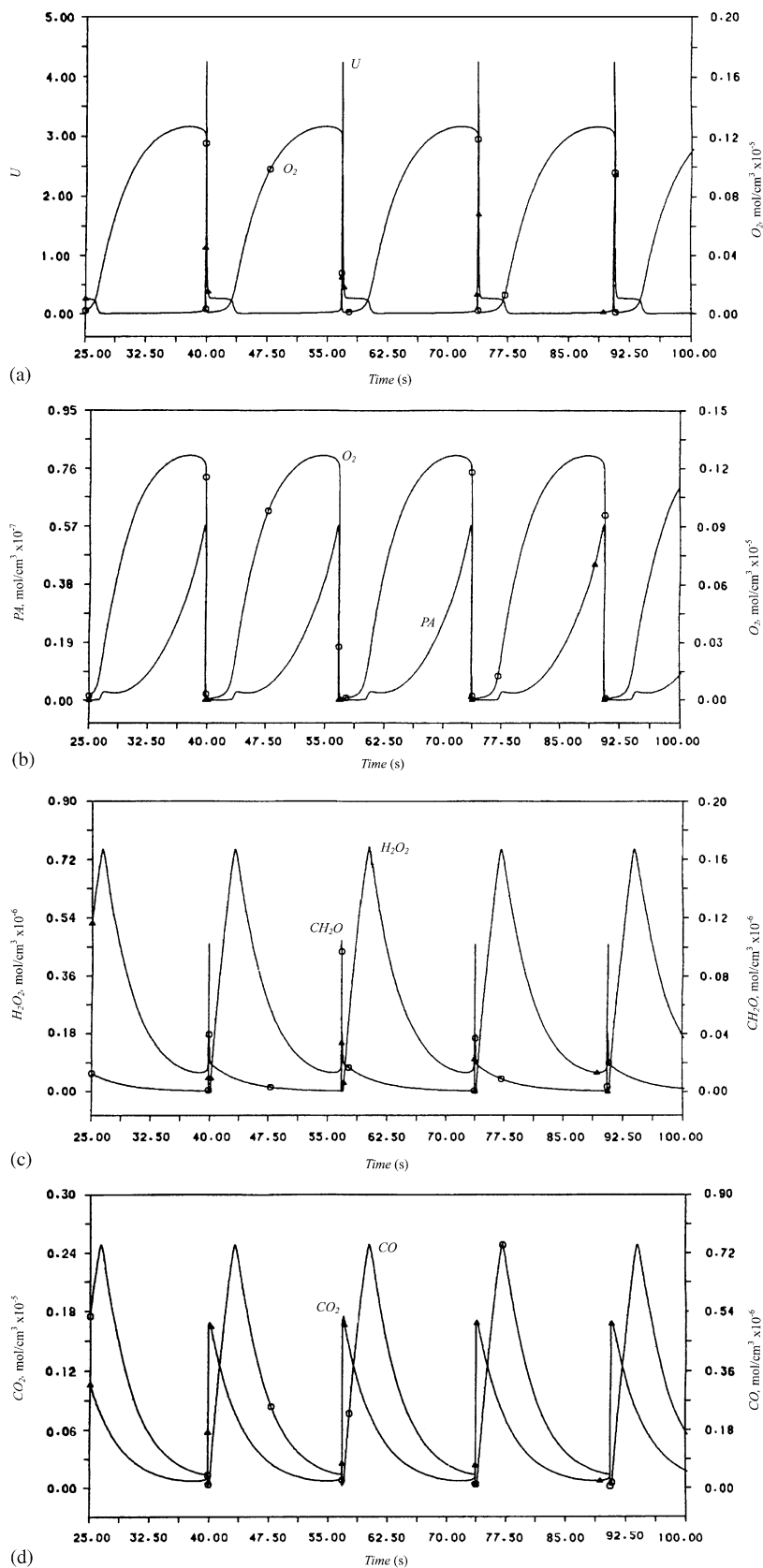


Fig. 7. Time evolutions of temperature and species at $P = 100$ Torr, $T_0 = 570$ K and $\tau = 4$ s (Regime II): (a) U and concentration of O_2 , (b) concentrations of O_2 and peracetic acid, (c) concentrations of H_2O_2 and CH_2O , (d) concentrations of CO and CO_2 .

concentration of CO_2 occurs after the thermal ignition further confirms this scheme.

After $[\dot{\text{H}}]$ has increased to a certain level and before O_2 is completely exhausted, reaction (W14) proceeds, causing $[\dot{\text{H}}\text{O}_2]$ to reach its maximum and causing CH_3CHO to become completely exhausted. (Note: this observation differs from the cool flame, where HO_2 maximizes *before* rather than *after* the cool flame). When the concentration of CH_3CHO increases further, reaction 15 occurs, leading to maximum H_2O_2 concentration (Fig. 7c).

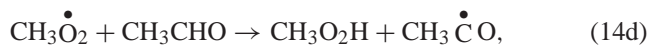
The above discussions address the reasons why CH_2O peaks before ignition, while H_2O_2 peaks after ignition. Since both CH_2O and H_2O_2 are largely exhausted during ignition, the role of H_2O_2 should also be considered in detailed modeling, just as CH_2O is considered.

Reaction (W16) has high activation energy and is endothermic in nature, and thus only proceeds at high temperatures. When the temperature reaches a high level but thermal ignition has not yet occurred, the $\dot{\text{O}}\text{H}$ radicals are formed using reaction (W16), yielding maximum concentration of $\dot{\text{O}}\text{H}$. The pool temperature decreases following ignition. Since H_2O_2 is stable at low temperatures (Cox and Cole, 1985), $[\text{H}_2\text{O}_2]$ maximizes following ignition. The O_2 , $\text{CH}_3\text{CO}_3\text{H}$ (Figs. 7a and b) and other intermediates are completely exhausted after thermal ignition, and thus the combustion during ignition oscillation is complete.

4. Discussions

The present simulation results confirm that the Wang–Mou scheme (Table 1) gives the stoichiometric balances of Regimes I and V, which differ from the experimental findings. Moreover, experiments have found H_2O to appear in large quantities in both Regimes I and V. The Wang–Mou scheme predicts that H_2O only appears in the thermal ignition stage in Regimes II and III using reaction 11. (Note: In Regimes I and V the temperature is too low for reaction 11 to be significant). Additionally, both CH_4 and CH_3OH are present in experiments, yet for simplicity the Wang–Mou scheme did not consider their formation. Conversely, the Wang–Mou scheme considers the formation of C_2H_6 and $\text{CH}_3\text{CO}_2\text{H}$, creating a discrepancy in the stoichiometric balance from experiments. Despite certain drawbacks, the present simulation correlates well with the dynamics of formation of CO and the exhaust of $\text{CH}_3\text{CO}_3\text{H}$ in the experiments.

Gibson et al. (1984) proposed a chemical model of oxidation of CH_3CHO , whose difference between the present model is the steps corresponding to the occurrence of cool flame. Their cool flame oscillation scheme includes:



Notably, reactions (14a) and (14b) form an equilibrium reaction. At high temperatures Eq. (14a) is preferred. That is, the chemical reaction favors the formation of $\text{CH}_3\dot{\text{O}}_2$ and the occurrence of Eqs. (14d) and (14e). At low temperature, the equilibrium prefers (14b), in favor of $\dot{\text{C}}\text{H}_3$. Gibson et al. (1984) claimed that reaction (14d) had low activation energy and was easy to proceed. However, experiments on acetaldehyde oxidation reveal no formation of $\text{CH}_3\text{O}_2\text{H}$. Moreover, the activation energy of reaction (14e) is rather high. Re-stated, $\text{CH}_3\text{O}_2\text{H}$ is relatively stable, which should not be an essential species in reaction. In Wang–Mou scheme the cool flame is induced by reactions (1–8) using $\text{CH}_3\dot{\text{C}}\text{O}$ as the branching carrier. Such a conclusion correlates with previous investigations (Blanchard et al., 1957; Halstead et al., 1971; Pugh et al., 1987).

Skrumeda and Ross (1995) measured the evolutions of species of CH_3CHO , CO_2 , H_2O , O_2 , CH_3OH , CH_2O , H_2O , and CH_4 in the cool flame regime. The phase lags (therein termed the “relative phase”) of CH_3CHO , H_2O_2 , O_2 , CH_3OH , CH_2O , CH_4 , hydroxyl radicals, and temperature were measured and compared with the outputs of two models: Pugh et al. (1987) (PR model) and Gibson et al. (1984) (GGGH model). The relative phases of the species in the Wang–Mou scheme are calculated and compared with the experimental data from Skrumeda and Ross (1995) in Table 4. Expect for H_2O_2 , the relative phase shifts of the other species in the highly simplified Wang–Mou scheme correlate with the experimental findings. Meanwhile, neither the more detailed PR model nor GGGH model could predict the relative phase of H_2O_2 .

The two-stage branching in the Wang–Mou scheme resembles that for Gibson et al. (1984), except for the following step assumed in the latter model



The reaction is endothermic and exhibits high activation energy, which should be unimportant in the thermal ignition. The Wang–Mou scheme excluded the role of $\dot{\text{O}}$.

Reaction (W15) in Table 1 only proceeds after thermal ignition, which corresponds to the maximum $[\text{H}_2\text{O}_2]$. At ignition H_2O_2 is completely decomposed to the free radical $\text{H}\dot{\text{O}}$ (reaction W16), as proposed by Gibson et al. Nevertheless, not as interpreted in this work, Gibson et al. (1984) further assumed the reaction between $\dot{\text{O}}$ and CH_2O to occur as follows:



Table 4
Comparisons of the relative phase shifts for various species in experiments and in model predictions

Species	Phase shift (degrees)			
	Experimental (Skrumeda and Ross, 1995)	PR Mode (Pugh et al., 1987)	GGH Model (Gibson et al., 1984)	WM Model (Wang and Mou, 1985)
Temperature	270	225–265	235	240–270
O ₂	15–45	–10–10	0	0–30
H ₂ O ₂	–10–44	110–160	ca. 180	150–200
CH ₃ OH	85–185	NA	ca. 180	NA
CH ₂ O	140–180	ca. 180	235	150–200
CH ₄	150–200	ca. 180	NA	NA
OH	270	250–310	270	NA

The peak of CH₃CHO is used as the reference to calculate phase shift.

This difference makes difference from our simulation results on the evolution of [CH₂O]. Evolutions of the other species from both schemes are similar.

5. Concluding remarks

This work discussed the use of 16 elementary reactions proposed by Wang and Mou (1985) (Wang–Mou scheme) to describe the dynamic behavior of acetaldehyde oxidized in continuous-flow stirred tank reactor (CSTR). The Wang–Mou scheme was deduced from the comprehensive chemical reaction scheme by Kaiser et al. (1986) and other works. As Section 2 illustrates, the reaction (K2) denotes the initiation step; reactions (3), (K8), (K13) and (K15) represent the low-temperature branching steps; reaction (4) is the low-temperature termination step; reactions (K12) and (K102) are high-temperature termination steps; and reactions (5–9), (K6), (K54) and (K79) correspond to the high-temperature branching steps.

Numerical simulations were then conducted on the 19 mass and energy balance equations that resulted. The five regimes of distinct chemical dynamics reported in the literature were noted in simulations, with superior agreement than the skeleton Wang–Mou model with the experimental findings. In Regime I (550 K), the major products were CH₃CO₃H, C₂H₆, CO₂, H₂O₂, CO, and CH₃CO₂H, and a small amount of H₂O. Meanwhile, the major products in Regime V (640 K) were CO, CO₂, H₂O₂, C₂H₆, a small amount of CH₃CO₂H, and trace of CH₃CO₃H. The change in CH₃CO concentration correlates closely with the evolution of pool temperature in the cool flame and ignition oscillation, which correlates with the species x in the Wang–Mou model. Meanwhile, CH₂O is the precursor of thermal ignition. Despite suffering certain drawbacks, the present simulation correlates well with the experimentally observed dynamics of CO formation and CH₃CO₃H exhaust.

Acknowledgements

The authors are grateful to National Science Council, ROC for financial support.

References

- Banerjee, I., Ierapetritou, M.G., 2003. Development of an adaptive chemistry model considering micromixing effects. *Chemical Engineering Science* 58, 4537–4555.
- Blanchard, L.P., Farmer, J.B., Ouellet, C., 1957. An investigation of the gas-phase oxidation of acetaldehyde by means of a rapid-scanning mass spectrometer. *Canadian Journal of Chemistry* 35, 115–123.
- Cavanagh, J., Cox, R.A., Olson, G., 1990. Computer modeling of cool flames and ignition of acetaldehyde. *Combustion and Flame* 82, 15–39.
- Chang, P.C., Mou, C.Y., Lee, D.J., 1996. Micromixing effects in a stirred tank: the random replacement IEM model. *Chemical Engineering Science* 51, 2601–2606.
- Chang, P.C., Mou, C.Y., Lee, D.J., 1999. Macromixing and micromixing effects on oscillations of apparent chemical reaction rates. *Journal of Physical Chemistry A* 103, 5485–5489.
- Cox, R.A., Cole, J.A., 1985. Chemical aspects of the autoignition of hydrocarbon–air mixture. *Combustion and Flame* 60, 109–123.
- Di Mao, F.P., Lignola, P.G., Talarico, P., 1993. Thermokinetic oscillations in acetaldehyde CSTR combustion. *Combustion and Flame* 91, 119–142.
- Felton, P.G., Gray, B.F., Shank, N., 1976. Low temperature oxidation in a stirred flow reactor II acetaldehyde (theory). *Combustion and Flame* 27, 363–376.
- Gibson, C., Gray, P., Griffiths, J.F., Hasko, S.M., 1984. Spontaneous ignition of hydrocarbons and related fuels: a fundamental study of thermokinetic interactions. In: *Proceedings of the 20th International Symposium on Combustion*, The Combustion Institute, Pittsburg, PA, pp. 101–109.
- Gray, P., Griffiths, J.F., Hasko, S.M., Lignola, P.G., 1981a. Oscillatory ignitions and cool flames accompanying the non-isothermal oxidation of acetaldehyde in a well stirred flow reactor. *Proceedings of the Royal Society of London. Series A, Mathematical and Physical Sciences* 374, 313–339.
- Gray, P., Griffiths, J.F., Hasko, S.M., Lignola, P.G., 1981b. Novel, multi-stage ignitions in the spontaneous combustion of acetaldehyde. *Combustion and Flame* 43, 175–186.
- Griffiths, J.F., 1995. Reduced kinetic models and their application to practical systems. *Progress in Energy and Combustion Science* 21, 25–107.
- Griffiths, J.F., Sykes, A.F., 1989. Numerical studies of a thermokinetic model for oscillatory cool flame and complex ignition phenomena in ethanol oxidation under well-stirred flowing conditions. *Proceedings of the Royal Society of London, Series A, Mathematical and Physical Sciences* 422, 289–310.
- Halstead, M.P., Prothero, A., Quinn, C.P., 1971. A mathematical model of the cool-flame oxidation of acetaldehyde. *Proceedings of the Royal Society of London. Series A, Mathematical and Physical Sciences* 322, 377–403.

- Halstead, M.P., Prothero, A., Quinn, C.P., 1973. Modeling the ignition and cool flame limits of acetaldehyde oxidation. *Combustion and Flame* 20, 211–221.
- Harrion, A.J., Cairine, L.R., 1988. The development and experimental validation of a mathematical model for predicting hot-surface autoignition hazards using complex chemistry. *Combustion and Flame* 71, 1–21.
- Hsu, T.J., Mou, C.Y., Lee, D.J., 1994. Effects of macromixing on the Belousov–Zhabotinsky reaction in a stirred reactor. *Chemical Engineering Science* 49, 5291–5305.
- Hsu, T.J., Mou, C.Y., Lee, D.J., 1996. Macromixing effects on Gray–Scott model in a stirred tank. *Chemical Engineering Science* 51, 2589–2594.
- Kaiser, E.W., Westbrook, C.K., Pitz, W.J., 1986. Acetaldehyde oxidation in the negative temperature coefficient sensitivity analysis of autonomous oscillations. Separating of secular terms and determination of structural stability. *International Journal of Chemical Kinetics* 18, 655–688.
- Lee, D.J., Chang, P.C., Mou, C.Y., 1997. Micromixing effects on autocatalytic reactions in a stirred tank: the random replacement IEM model. *Journal of Physical Chemistry* 101, 1854–1858.
- Liang, C.H., Mou, C.Y., Lee, D.J., 2003. Dynamic behavior and sensitivity of skeleton thermokinetic model for acetaldehyde oxidation. *Chemical Engineering Science* 58, 4173–4184.
- Pugh, S.A., Kim, H.R., Ross, J., 1987. Measurements of [OH] and [CH₃CHO] oscillations and phase relations in the combustion of CH₃CHO. *Journal of Chemical Physics* 86, 776–783.
- Scott, S.K., 1991. *Chemical Chaos*. Cambridge University Press, Cambridge.
- Sirdeshpande, A.R., Ierapetritou, M.G., Androulakis, I.P., 2001. Design of flexible reduced kinetic mechanisms. *A.I.Ch.E. Journal* 47, 2461–2473.
- Skrumeda, L.L., Ross, J., 1995. Further measurements on the oscillatory cool flame oxidation of acetaldehyde and comparison with reaction mechanism models. *Journal of Physical Chemistry* 99, 12835–12845.
- Vardanyan, I.A., Nalbandydn, A.B., 1985. Advances in the study of the mechanism of the gas-phase oxidation of aldehydes. *Russian Chemical Reviews* 54, 532–543.
- Wang, X., Mou, C.Y., 1985. A thermokinetic model of complex oscillations in gaseous hydrocarbon oxidation. *Journal of Chemical Physics* 83, 4554–4561.
- Westbrook, C.K., Dryer, F.L., 1984. Chemical kinetic modeling of hydrocarbon combustion. *Progress in Energy and Combustion Science* 10, 1–57.
- Yang, C.H., Gray, B.F., 1969a. On the slow oxidation of hydrocarbon and cool flames. *Journal of Physical Chemistry* 69, 3395–3406.
- Yang, C.H., Gray, B.F., 1969b. Unified theory of explosions, cool flames and two stage ignitions, part 2. *Transactions of the Faraday Society* 65, 1614–1622.